Article

Collapse of a Confined Polyelectrolyte Chain under an AC Electric Field

Keerthi Radhakrishnan* and Sunil P. Singh*

Read Online

ACCESS | Metrics & More | Article Recommendations | Supporting Information

ABSTRACT: Field-driven transport through nanofluidic devices has emerged as one of the promising tools for characterizing the conformational and dynamical response of long polyelectrolytes (PEs). We investigate a PE chain's structural dynamics confined within a cylindrical channel subject to a square-wave AC field using hybrid coarse-grained molecular dynamic simulations coupled with a particle-based mesoscopic simulation method that captures long-range hydrodynamic interactions (HIs). In the weak-field limit, stretching of the chain is observed, followed by a substantial shrinkage beyond a critical field strength when the applied field's time period is comparable to the chain's intrinsic relaxation in a DC field. Closer insights reveal two main facets; (i) the indispensability of the HIs and (ii) multiple backfolded domains in the form of hairpin effectuates overall shrinkage of the chain. We retrieve this non-monotonic structural response of the chain using an empirical expression involving local stretching, number of folded domains, and its size. Additionally, we elucidate key aspects such as the role of confinement, the chain's degree of ionization, mobility of adsorbed ions, polarization, global persistence length, and their variation with the applied field strength and frequency.
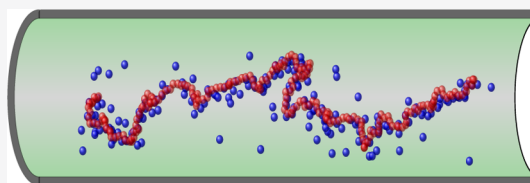
1. INTRODUCTION

The last couple of decades have seen an upsurge in nanofluidic-based technologies, which allow manipulation of the structural and transport behavior of various bio-polymers.[1−13] In particular, nanochannel electrophoresis has been leveraged extensively in the characterization of artificial gels,[14] separation of long polyelectrolytes (PEs),[6,7] and identification of DNA sequences.[5−11] The electrophoretic response of a homogeneously charged PE[7,15] is rather intriguing due to the electrostatic and hydrodynamic coupling of counterion cloud with the chain, unveiling unusual transport behaviors such as molecular-weight-independent mobility of longer chains,[7,16] non-monotonic mobility of shorter chains,[17−20] and other counterintuitive structural responses.[21,22] Along with the multi-scale coupling of PE in bulk, the presence of strong spatial confinement brings further addendum to its characteristic features such as elongation,[23−27] suppression of diffusion,[28−30] cross-streamline migration,[31,32] and mobility reversal.[33] Strong temporally varying fields may lead to further behavioral complexities as exemplified in recent experiments,[34−36] where a DNA molecule undergoes large-scale structural collapse in an AC field. However, the broader consensus is that a PE chain stretches under a homogeneous field as reported in several electrophoresis experiments[23,37−39] and simulation studies.[18,24,40−42]

A theoretical proposal attributes the structural collapse of DNA under the AC field to the polarization attraction between folded domains,[43] while another one emphasizes the attraction between polarized density fields.[36] These models present plausible arguments for the chain compression; however, there is no clear understanding from the microscopic perspective of

what physics governs such a large-scale conformational transition.

Previous simulation studies of PEs in bulk predominantly focus on the low-frequency regime, where the time-period of the AC field τ_ν is longer than the equilibrium relaxation time $\tau_{R_e}^0$ of the PE.[24,40−42] Also, a comprehensive study of the confined PE under the AC field in the presence of hydrodynamic interactions (HIs) remains unprecedented.[40,41] Following this, in this article, we elucidate the role of a spatially homogeneous square-wave AC field on the conformational dynamics of a confined PE at frequency $\tau_\nu < \tau_{R_e}^0$. Here, we use coarse-grained hybrid molecular dynamics simulations coupled with multi-particle collision dynamics (MPC) to account for long-range HI.

Our key findings are enlisted herein; the PE beyond a critical field strength undergoes a field-induced compression within a frequency range. A plausible origin of this frequency dependence lies in the relaxation timescales associated with the chain under DC fields. Our results confer further clarity regarding the inevitability of HIs along with moderate confinement in transverse directions in attaining the chain collapse. A universal scaling procured for the PE structural response with E^2/ν (where E is the field strength and ν is the frequency)[34] further

corroborates the primary role of field-induced hydrodynamic flow[44] in the chain's compression. Moreover, structural insights obtained indicate that the collapse is anisotropic in nature due to the occurrence of hairpin-like folded domains, with a sheer resemblance to Odijk's backfolding of a confined semiflexible chain in equilibrium.[26,45] The backfoldings seen in semiflexible chains span a narrow window of confinement $2R_p \approx l_p$; however, our results show that an AC field can instigate such foldings in PEs even for moderate confinement regimes pertaining to $R_p \approx R_g^0$. Here, l_p is the persistence length, R_p is the pore radius, and R_g^0 is the radius of gyration of the PE in bulk. Further, the scope of work encapsulates the dynamical coupling of counterions to the chain in response to the applied field. Our results indicate a non-monotonic variation in the adsorbed ions' mobility with the field due to its strong coupling with the chain's folded conformations. Moreover, field-orchestrated ion reorientations lead to linear polarization in the limit of a strong field with a universal dependence on E/ν.

The article here is organized in the following way: Section 2 pertains to the simulation model used for the PE and the solvent. In Section 3, we present results of our simulations further categorized into five different subsections. Finally, in Section 4, we summarize and conclude the results of the manuscripts.

2. SIMULATION MODEL

The PE is modeled as a bead-spring chain comprising N monomeric units with uniform charge $q = -e_0$ assigned to each bead, where e_0 is a unit charge. Also, N counterions possessing an opposite charge $q = +e_0$ are introduced in the solution. Various kinds of interaction among monomers and ions are implemented using $U = U_s + U_{LJ} + U_e + U_w$, where U_s accounts for the chain connectivity, U_{LJ} accounts for the excluded volume, U_e accounts for the electrostatics, and U_w accounts for the confinement. The chain connectivity is secured by harmonic spring potential U_s given as $U_s = \frac{1}{2}\kappa_s \sum_{i=1}^{N-1}(|\mathbf{r}_{i+1} - \mathbf{r}_i| - l_0)^2$, where $\mathbf{r}_i$ is the position vector of a particular bead, l_0 is the equilibrium bond length, and κ_s is the spring constant. A standard repulsive Lennard-Jones (LJ) potential U_{LJ} is used among all monomers and counterions[25] with the interaction energy $\epsilon_{LJ}/k_BT = 1$ and diameter $\sigma/l_0 = 0.8$.

The electrostatic interaction among the charged molecules are taken into account via the Coulomb potential $U_e = \sum \frac{l_B k_B T}{r_{ij}}$, where r_{ij} is the distance between a pair i and j and summation is over all the pairs in the primary simulation box along with its periodic images. Here, Bjerrum length l_B is basically the length at which the electrostatic interaction energy of an ion is comparable to its thermal energy. In our simulations, we adhere to $l_B = 3.0$ as many biological polymers such as dsDNA typically span the range of 2−4 in the solution.[7] The boundary wall considered here is electrically neutral. The effect of cylindrical confinement (see Figure 1) is materialized using repulsive LJ
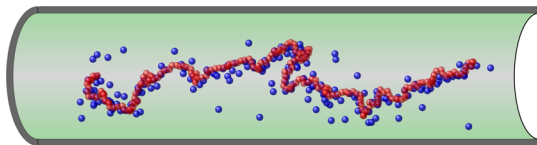

Figure 1. PE chain (red) and counterions (blue) inside a cylindrical channel. Only a portion of the tube is shown for a better resolution of the ions and the chain.

potential U_w imposed between the wall and the molecules (monomers and counterions), with the energy parameter $\epsilon_w/k_BT = 1$ within a cut-off distance of $2^{1/6}(\sigma/2)$ from the wall.

All the charged molecules are subjected to a square-wave AC field that imposes a force $F_e^i = \text{sign}[\sin(2\pi\nu t)]q_i E$ on the ith molecule directed along the channel axis, where ν (time period, $\tau_\nu = 1/\nu$) and E stand for the frequency and amplitude of the field, respectively. There are various approaches for the electrostatic force calculations for the cases of slab and tube geometries with a finite boundary in one or two directions.[46−50] These techniques are computationally very expensive because of the occurrence of double summation over particles in the reciprocal space unlike the conventional 3D-Ewald summation.[51,52] Following this, to estimate the electrostatic interactions in a confined system, we employ a simplified description of the Ewald summation with the assumption of periodicity in all directions.[47,48] Here, we have an infinite space of periodically arranged cylinders such that the region of empty space separating the tubes in confined directions is sufficiently large to ensure negligible effect of periodic images on the system interactions. Following this, in the confined directions, the periodic boxes L_y and L_z are chosen such that they satisfy the condition $(L_y, L_z) > R_p$.[47,48] Here, R_p is the pore radius and L_y, L_z are the simulation box lengths in lateral directions. This assumption of periodicity in lateral directions in our case is validated by spanning a whole range of varying L_y, L_z (see Supporting Information Figure S5[53]) such that the chain's structural response remains invariable to the choice of periodic box length in the confined directions.

For simplicity, electric permittivities of the medium and the pore are assumed to be the same throughout. The details of solvent dynamics within the framework of MPC[25,31,54−58] and its coupling with molecular dynamics is presented in the Supporting Information in the MPC section.[53] This technique encapsulates thermal fluctuations and long-range HI, which are crucial for the study of most of the soft-matter systems.[54,55]

2.1. Simulation Parameters. All parameters are measured in reduced MPC simulation units; cell length a, solvent mass m, and thermal energy k_BT. The integration of equation of motion of chain and ions is performed via the velocity Verlet algorithm with a step size of $h = 0.005\tau$, where $\tau = a(m/k_BT)^{1/2}$.[59,60] The parameters associated with the MPC fluid are average solvent particles per cell $\langle N_c \rangle = 10$, rotation angle $\alpha = 130°$, collision time step $h_c = 0.1\tau$, and shear viscosity $\eta = 8.7\sqrt{mk_BT}/a^2$. These parameters correspond to the diffusion constant of a free-ion $D_0 \approx 0.02$. The parameters for the PE are spring constant $\kappa_s = 10^4$, bond length $l_0/a = 1$, mass of the monomer $M = 10m$, chain length L, and box length L_x such that $L = L_x = Nl_0$. The periodicity in confined directions for the Ewald summation are taken as $L_y = L_z = 100$. The number of monomers and pore radius are always taken to be $N = 200$ and $R_p = 10$, respectively, unless specified otherwise, in which case R_p/a ranges from 8 to 20. The chain's electrostatic persistence length is $l_p \approx 2$ for the chosen set of parameters.

The choice of field strength lies in the range 0−5 and frequencies 0.001−0.05. However, the equilibrium relaxation time of the chain end-to-end fluctuations is $\tau_{R_e}^0 \approx 9000$, and the lowest time-scale associated with the diffusive length-scale of a free ion sized σ is $\tau_D = \sigma^2/D_0 \approx 32$, where D ≈ 0.02. The choice of the frequency in the present context lies within a window $\nu = 1/\tau_\nu$: 0.001−0.05 such that ν is always smaller than the

relaxation time of the chain and larger than the diffusive time-scale $1/\tau_D$.

In order to map this chosen frequency window onto actual experimental realizations of confined chains, we simply normalize it relative to the chain's intrinsic relaxation time $\tau_{R_e}^0$.

This dimensionless metric is given as $\nu\tau_{R_e}^0$, which renders a value between 9 and 450 for the corresponding chosen frequency of ν: 0.001−0.05; for example, a 21 μm λ-DNA which has an experimentally available relaxation time of 0.4 s[61] inside a channel in a moderately confined de Gennes regime of $2R_p/l_p \approx$ 10.[62−64] Our range of frequency $\nu\tau_{R_e}^0$: 9−450 then roughly corresponds to the experimental window of ν: 20−1100 Hz for λ-DNA, which approximately overlaps the range of 100−700 Hz reported in the experiments on DNA collapse in AC fields.[34,36]

3. RESULTS

3.1. Conformation of PE. The mean extension of the PE chain is parametrized using standard quantities of a polymer such as the average radius of gyration and end-to-end distance given as $R_g = \sqrt{\left\langle \frac{1}{N}\sum_{i=1}^{N}(\mathbf{r}_i - \mathbf{R}_{cm})^2 \right\rangle}$ and $R_e = \sqrt{\langle(\mathbf{r}_1 - \mathbf{r}_N)^2\rangle}$, respectively, where $\mathbf{R}_{cm}$ is the center-of-mass of the chain. The normalized values of R_g and R_e w.r.t. the corresponding equilibrium values for varying field strengths and frequencies are presented in Figure 2a.
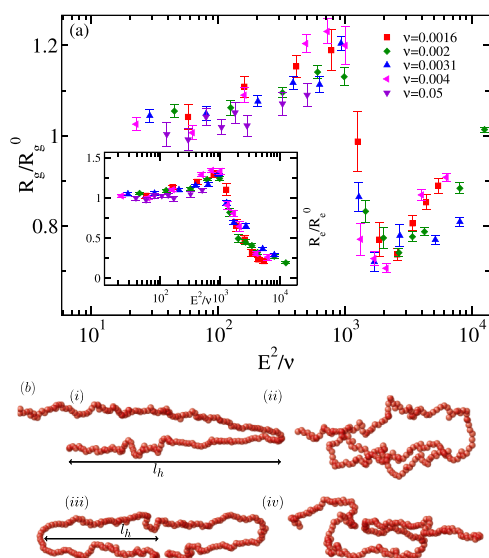

Figure 2. (a) Variation of R_g/R_g^0 of the confined chain as a function of E^2/ν at varying frequencies. The inset shows the relative variation of R_e/R_e^0 as a function of E^2/ν for various frequencies as shown in the main plot. The critical field $E_c \approx 1.1$, 1.4, 1.7, 2 for $\nu = 0.0016$, 0.002, 0.003, and 0.004, respectively. (b) Various conformations of the PE in the compressed state are depicted having one (i), two (ii), two (iii), and four (iv) hairpins, respectively.

It is evident from the plot that for frequencies $\nu = 0.001−$0.004, the chain exhibits a gradual stretching with increasing field strength in the weak field regime, that is, $E^2/\nu < 10^3$. However, beyond a critical field E_c at which $E^2/\nu \approx 10^3$, a sharp and substantial shrinkage in the chain size is observed. This compression behavior only pertains to a narrow window of E as the chain again swells with further increase in field strength. The maximum reduction in R_g accounts for roughly 30% of its

equilibrium value, while for R_e, it reaches up to 75%. The pronounced reduction in R_e indicates that the chain attains a folded conformation where the terminal ends come close together. A few snapshots of the inherent PE conformations are illustrated in Figure 2b, and corresponding movies for the collapsed and stretched states are also shown in the Supporting Information Movies S1 and S2.[53] For the case of $\nu = 0.05$ (which is $\nu \approx 1/\tau_D$), the chain is weakly perturbed from its equilibrium conformations despite being exposed to the same range of electric field of 0−5. A plausible explanation for this is as $\nu \to 1/\tau_D$, that is, free ion's diffusive timescale, the monomers and counterions are not allowed to respond to the applied field adequately. As a result of this, at very high frequencies $\nu \gg 1/\tau_D$, the chain conformations remain nearly unperturbed despite large fields.

The drift of macromolecules under the AC field induces hydrodynamic flow fields in the channel. It is pre-established through an electrohydrodynamic theory, primarily derived for DNA aggregations,[44] that the strength of this field-induced flow is proportional to $(E^2/\nu)^2$. Notably, similar scaling is reported in prior experimental studies on DNA compression under an AC field,[34] where they procured a universal curve for the chain's response with E^2/ν. Following their proposition, we present particularly the structural response as a function of E^2/ν. Interestingly, all the curves pertaining to R_g/R_g^0 and R_e/R_e^0 superimpose on each other, displaying a universal behavior with E^2/ν, hence emphasizing the importance of the underlying HIs. The inevitability of HIs in the compression of a chain is further corroborated by simulations done explicitly without HIs for the same solvent viscosity $\eta_s = 8.7$. The results are shown in Figure 3. The main plot shows the variation in radius of gyration
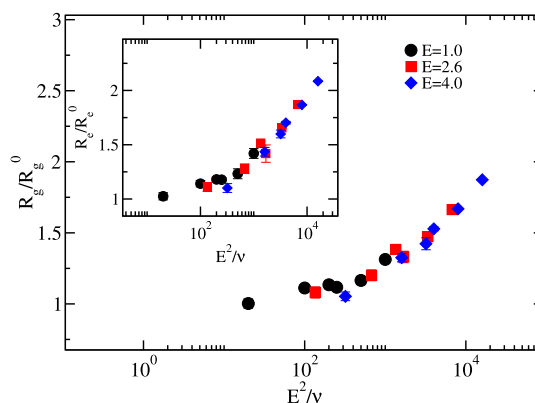

Figure 3. Variation in normalized radius of gyration R_g/R_g^0 of the confined chain without HIs as a function of E^2/ν for various field strengths for the chain length $N = 200$. The inset shows the variation in normalized end-to-end distance R_e/R_e^0 for the same set of field strengths shown in the main plot. Here, $R_g^0 \approx 23.7$ and $R_e^0 \approx 73$ correspond to the equilibrium values of radius of gyration and end-to-end distance, respectively, of $N = 200$ inside the channel of radius $R_p = 10$.

R_g as a function of E^2/ν, where individual curves pertain to specific field strengths varied over a range of frequencies. Evidently, in the absence of HIs, the chain exhibits a monotonic stretching over a range of varying E^2/ν and is devoid of any shrinkage quite contrary to the case where HI is present (see Figure 2a).[40] Similar increase in chain end-to-end distance R_e with the field is seen in Figure 3 (inset), which otherwise manifests a substantial drop in its value due to chain ends coming close together through folding.

Another crucial aspect is to ascertain the influence of degree of confinement on the present phenomenology, especially in the wake of possible hydrodynamic coupling between the chain and the confining walls. The response of the PE chain obtained for various confinements ranging from $R_p/R_g^b \approx 0.3$ to $R_p/R_g^b \approx 0.8$ in the presence of a field with varying strengths and a fixed frequency $\nu = 0.002$ is shown in Figure 4. The chosen range of
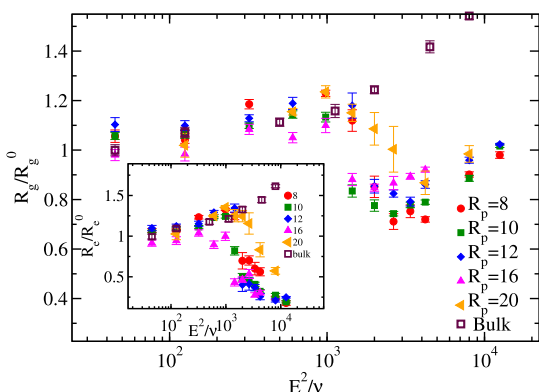

Figure 4. Variation in the normalized radius of gyration R_g/R_g^0 of a chain with E^2/ν at $\nu = 0.002$ for different pore radii R_p. Here, R_g^0 pertains to the equilibrium value ($E = 0$) for the corresponding confinements. The open symbol (square) corresponds to the stretching of the chain in the bulk for $N = 200$, $\nu = 0.002$, and $L_x = 200$, $L_y = 60$, $L_z = 60$ (without confining walls). The inset displays the variation of R_e/R_e^0 with E^2/ν at $\nu = 0.002$ for pore radii mentioned in the main plot.

confinement R_p/R_g^b: 0.3−0.8 fairly spans the moderately confined de Gennes regime[62−64] (where $R_p \sim R_g^b$). Here, $R_g^b \approx 25$ stands for chain's radius of gyration in bulk for $N = 200$. It is evident that for a sizably small pore radius, that is, $R_p/R_g^b \approx 0.3$ ($R_p = 8$), the chain exhibits substantial shrinkage beyond the critical field E_c. Further, as the pore radius increases from R_p: 8−20 such that $R_p \rightarrow R_g^b$, the extent of compression exhibits a pronounced reduction. For example, at $R_p = 8$, R_g is maximum reduced by 30% (see Figure 4 in bullets) from its equilibrium value. On the other hand, this compression lowers down to nearly 10% for the case of $R_p = 20$. Nonetheless, the critical field E_c exhibits a weak dependence on R_p. Additionally, we undertook explicit simulations for the bulk case, with no confining walls present for a range of varying field strengths at the frequency $\nu = 0.002$ (shown in open symbols in Figure 4). Interestingly, in bulk, the PE chain exhibits monotonic stretching with increasing E in lieu of shrinkage. This emphasizes the inevitability of confinement in lateral dimensions ($R_p \sim R_g^b$) in effectuating chain collapse.

Additionally, we analyze the chain length dependence of the PE collapse mechanism, where we characterize the inflexion point as the critical field, as done in past studies.[40,65] Considering that the collapse is observed only beyond a certain E_c and within a window of frequencies, we choose a frequency $\nu = 0.004$ for which $N = 125, 150, 175,$ and 200 all show chain shrinkage. Following this, Figure 5 shows the variation in R_g/R_g^0 for the chain lengths mentioned above. In order to find the qualitative behavior of E_c on N, we rescale x-axis (E^2/ν) in the plot by a chain length-dependent factor. All the curves nearly superimpose on each other in the transitional region if the x-axis is presented as $(EN)^2/\nu$. Here, we retrieve the critical field's behavior as $E_c \sim N^{-1}$, which infers a decrease in E_c with increasing chain length. This is qualitatively in accordance with
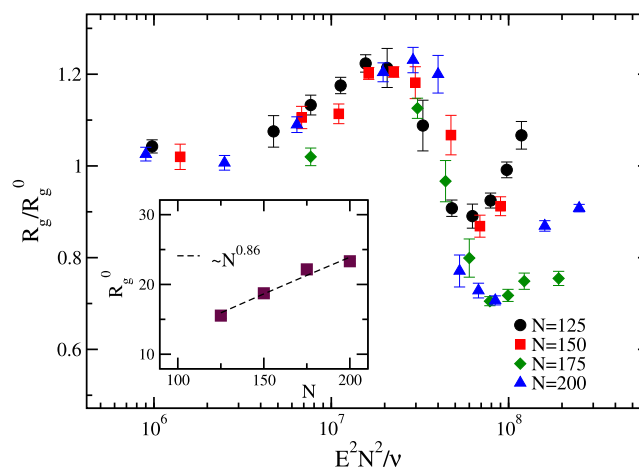

Figure 5. Variation in the normalized radius of gyration R_g/R_g^0 with $(EN)^2/\nu$ for various chain lengths $N = 125, 150, 175,$ and 200. The inset shows the variation in R_g^0 with the chain length in confinement for pore radius $R_p = 10$, which gives the swelling exponent $\nu_p \sim 0.86$.

the scaling of $E_c \sim N^{-3\nu_p/2}$ (where ν_p is the swelling exponent) reported in prior studies on PE stretching/unfolding under DC[42] and AC[40,65] electric fields. Given that $\nu_p \approx 0.86$ in our case (see the inset of Figure 5), we get roughly $E_c \sim N^{-3\nu_p/2} = N^{-1.3}$, which indicates a comparatively stronger dependence on the chain length than the one obtained in our simulations. The difference in the exponent obtained here for E_c is possibly because the previous studies under AC fields were carried out in a low-frequency regime,[40,65] where the time period of the applied field is much larger than the chain's relaxation time such that complete relaxation of ions and the chain in response to the field is allowed. Hence, it renders similar scaling seen in DC, unlike our case involving a high-frequency field. Apart from this, we speculate that the presence of shorter chain lengths, confinement, and hydrodynamics might also influence the obtained N dependence.

In summary, the structural folding mechanism observed in the present context shares phenomenological similarities with certain other systems such as elastic rods,[66] where the strong field-induced in-homogeneous hydrodynamic drag across the chain leads to hairpin-like structures. This further extends to the cases involving other kind of fields such as shear-flow and sedimentation,[21,22,66−68] where structural compaction of the neutral chains is reported. Unlike the aforementioned cases where homogeneous compaction of the chain is seen, folding in PE possibly occurs due to intra-segmental repulsion. Additionally, for a PE under an AC field, the alternating nature of the field itself favors bidirectionality in segmental orientations, resulting in field-induced curvatures, facilitating the process of chain folding.[69]

3.2. Global Persistence Length. Structural analysis of the PE indicates that multiple folded domains across the contour cause overall shrinkage of the chain. These folds/bends are predominantly in the form of elongated U-shaped hairpins aligned along the channel axis. Such backfolded structures are quite prevalent in the case of semi-flexible chains under strong confinement, where $2R_p \approx l_p$.[26,27,70] Among several existing literature on confined polymers,[70−72] one of the reigning theories proposed by Odijk[26,73] shows that at much relaxed confinements ($2R_p \gg l_p$), the chain simply adheres to the de Gennes blob picture, while at extreme confinements ($2R_p \ll l_p$), a new length scale λ_D emerges, which is that fragment of the

chain beyond which the transverse undulations saturate to the channel diameter. These chain segments deflect back and forth between the walls. Hence, the chain as a whole can be viewed as a sequentially arranged array of these deflection segments. The crossover between the aforementioned limits is mediated by $2R_p \sim l_p$ regime, where these deflection segments have the propensity to backfold with a characteristic length g analogous to the 1-D self-avoiding random walk of a worm-like chain with l_p replaced by g. Here, g refers to the global persistence length in the backfolded state.[26,27,45,74] Interestingly, our choice of parameters $R_p/R_g \approx 0.4$ and $2R_p/l_p \approx 10$ indicates that the chain fairly spans the moderately confined de Gennes regime; despite that, the AC field drives the chain to the backfolded state.

Considering the analogy between a confined chain and the case of a nematically aligned semiflexible chain,[27,75,76] the mean extension $R_x{}^2$ of the backfolded chain can be written as

$$R_x{}^2 = \frac{1}{3}(1 + 2m)\{2gs - 2g^2(1 - \exp(-s/g))\} \tag{1}$$

where the expression resembles the case of a worm like chain (WLC) chain executing a 1-D random walk. The prefactor m accounts for the alignment of the chain along the field direction and s stands for the arc length ($s = l_0, 2l_0, ..., Nl_0$). The mean-extension of the chain is estimated as a function of arc-length.[27,74] Subsequently, a fit to estimate R_x is obtained using the aforementioned eq 1, with m and g as free parameters. The mean extension $3R_x{}^2/2gs(1 + 2m)$, normalized in terms of the procured values of m and g, is presented in Figure 6a. Evidently, the chain extension shows linear growth for $s/g < 1$ and is in accordance to Odijk's proposition of a chain exhibiting rod-like scaling at $s/g < 1$ in the backfolded state. The slump in $R_x{}^2$ in the region $s/g \gg 1$ is a manifestation of the chain foldings seen at characteristic length g. This is an inadvertent consequence of the chain extension R_x comparable to g. For the large chain lengths where $R_x \gg g$, the chain will exhibit expected real chain scaling.[27,74]

Further, the obtained g from eq 1 is presented in the inset of Figure 6a as it accounts for the size of the folded domains.[26,27,74] Here, expectantly the global persistence length grows with E, which can be understood in terms of the field-enhanced alignment of the bonds. Additionally, g follows a master curve when presented as a function of E/ν and exhibits a power-law $g \sim (E/\nu)^{2/3}$ in the backfolded regime. However, we expect for much larger fields that g will diverge, off-shooting the contour length, leading to a linear chain with no backfoldings.

Having established that the field induces stiffness along the chain at the length scale g, now, our emphasis herein is to decipher the local picture pertaining to the average alignment of bonds. The metric m used here for the alignment accounts for the angle between the field direction and tangent to the chain, expressed as

$$m = \frac{1}{N - 1}\sum_{i=1}^{N-1}\frac{3}{2}\left[\left(\frac{\mathbf{R}_{i,i+1}\cdot\mathbf{E}}{R_{i,i+1}E}\right)^2 - \frac{1}{3}\right] \tag{2}$$

From the definition, it is clear that $m = 1$ corresponds to a fully aligned chain, whereas $m = 0$ represents a completely isotropic case. The computed values in terms of $1 - m$ are depicted in Figure 6b. It shows that $1 - m$ undergoes a monotonic decrease with E/ν beyond a threshold E_c; conversely, the degree of alignment m grows in the compressed regime. This indicates that high field strengths not only induce chain folding globally
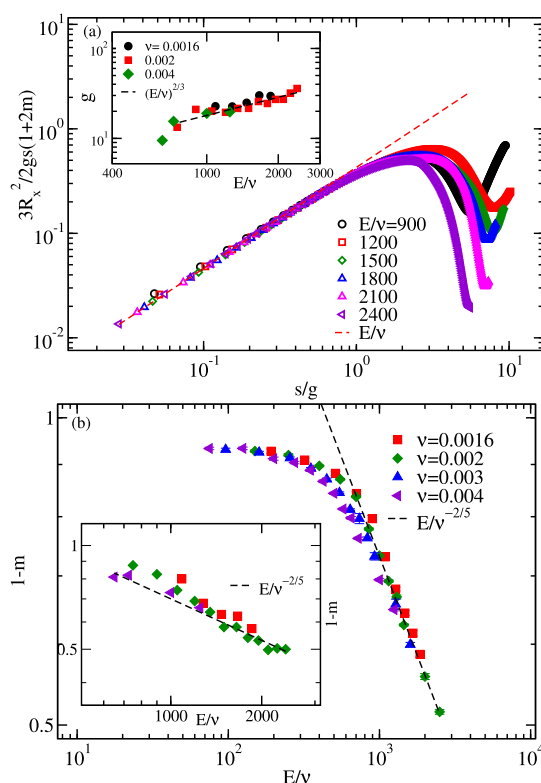

Figure 6. (a) Variation in the scaled extension $3R_x{}^2/(2gs(1 + 2m))$ with s/g for various E/ν as displayed in the plot. The behavior of the superimposed curves is nearly linear in the $s/g < 1$ region as traced by the red dashed line with slope unity. The inset shows the global persistence length obtained from the fitting done for $R_x{}^2$ using eq 1. The dashed line shows power law behavior of $g \approx (E/\nu)^{2/3}$. (b) Alignment parameter $1 - m$ with E/ν. The dashed line reflects the power-law behavior $(1 - m) \approx (E/\nu)^{-2/5}$ in the backfolded regime; here m is computed from eq 2. The inset shows $1 - m$ obtained from the best fit given in eq 1.

but also effectuate significant alignment of bonds along the field direction. Notably, $1 - m$ also exhibits the same universal behavior as E/ν, following a power-law scaling $1 - m \approx (E/\nu)^{-\delta}$ with $\delta \approx 2/5$ as illustrated in Figure 6b. The effect of field-induced alignment can be qualitatively retrieved by varying the degree of confinement for a semi-flexible chain in equilibrium,[27] where the dependence over E/ν is equivalent to $2R_p/l_p$ with a different scaling exponent. Moreover, for comparison, we have shown the alignment parameter m in the inset of Figure 6b obtained from eq 1. Impressively, it captures all the qualitative features of the main plot, including the growth of field-induced alignment following a power-law with an exponent of approximately 2/5 in the backfolded regime.

3.3. Characterization of Backfolding. In this part, we elucidate the local conformational details of the chain explicitly in terms of hairpin numbers and associated size. The estimated number of hairpin occurrences N_h along the chain as shown in Figure 7 (inset) displays a non-monotonic variation with field, where N_h sharply grows near E_c followed by a decrease for $E^2/\nu > E_c{}^2/\nu$. This drop in N_h for $E > E_c$ is possibly a manifestation of the finite chain length used such that when a hairpin grows sizably proportional to the chain dimensions, accommodating multiple such bends becomes sparse. This proposition is further corroborated by looking at the average hairpin length l_h (illustrated in Figure 2b), where E_c clearly marks the emergence of hairpin nucleation, followed by a continually increasing l_h with
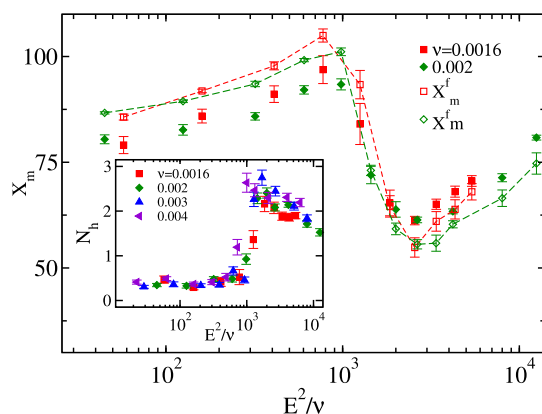
Figure 7. Comparison of average max-extension X_m plotted as a function of E^2/ν at frequencies of $\nu = 0.0016$ (squares) and 0.002 (diamonds). The filled symbols correspond to the values obtained from the simulations and open symbols are the values obtained from the proposed empirical expression $X_m^f = X_m^0(E) - N_h l_h$. The inset shows the variation in the number of hairpins N_h along the chain as a function of E^2/ν.

the field (Supporting Information Figure S2[53]). This estimated hairpin length l_h de facto shares a semblance to the global persistence length g presented in Figure 6a.

The average max-extension X_m of the chain estimated in terms of the hairpin variables $\{N_h, l_h\}$ predetermined for a few frequencies is presented in Figure 7. Here, $X_m = \langle|\max(r_i^x) - \min(r_j^x)|\rangle$, with i and j being the monomer index. To describe the characteristic features of X_m, we propose an empirical expression $X_m^f = X_m^0(E) - N_h l_h$, where X_m^0 stands for the average max-extension in the absence of any hairpins and $N_h l_h$ is a measure of the overall chain segment constituting the back-folded length within N_h hairpin domains. The latter is subtracted to account for the overlapping regions in the chain's mean extension calculation. Moreover, considering the fact that field-induced local chain alignment precedes the global folding, X_m^0 is expressed as $X_m^0 = N\delta x$ instead of the chain's equilibrium length. Here, $\delta x = \langle(r_i^x - r_j^x)\rangle/|j - i|$, with i and j being the monomer index, accounts for the induced local stretching and alignment of bonds along the field direction. This is exemplified in Figure 7 for $E < E_c$, where the chain devoid of hairpins undergoes a gradual stretching with the field. The proposed expression of X_m^f essentially captures all the characteristic features of the simulation results, both qualitatively and quantitatively.

3.4. Dynamics of Ions. In the purview of the structural and dynamical response of PE, the coupling of the counterion's dynamics with the chain has always been a fundamental quantity. To probe this, one can quantify the number of adsorbed ions N_c on the chain's surface that ascribes the PE's degree of ionization.[2,7,7,17,77,78] An ion is marked as adsorbed within a cut-off distance of $R_c = \frac{2}{3}l_B$ from any monomer,[2,17,25,77] where at R_c, the electrostatic energy of an ion-pair is comparable to its thermal energy. Figure 8 depicts the change in degree of ionization $\alpha = 1 - N_c/N$ obtained from the simulations with varying E and ν, renormalized to E^2/ν. Importantly, once again, a universal behavior for α is retrieved, where all the data merge nearly onto a single master curve. As expected, under subjection to field, desorption of counterions from the chain's backbone enhances, wherefore the chain's degree of ionization becomes a monotonically increasing function of E. For instance, at a large E
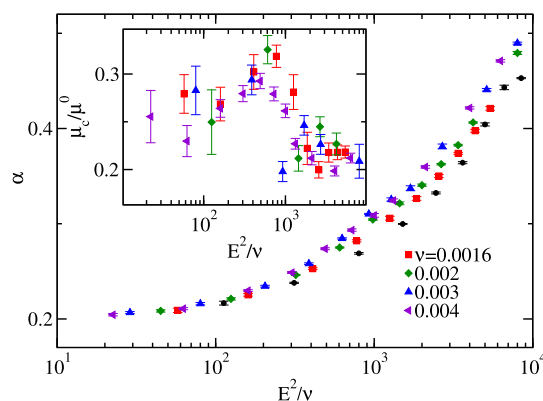

Figure 8. Variation in degree of ionization of the PE, $\alpha = 1 - N_c/N$, as a function of E^2/ν. The inset illustrates the variation in the adsorbed ion's mobility μ_c/μ^0, normalized w.r.t. to the free ion's mobility $\mu^0 \approx 0.015$ with E^2/ν.

(see Figure 8), the PE is nearly 50% ionized relative to that of 20% in equilibrium.

Furthermore, the dynamical coupling of the counterion with the PE can be examined by looking at the mobility, especially the adsorbed ion's mobility μ_c. Typically, μ_c is smaller than the mobility of a free ion because of the strong electrostatic coupling of the adsorbed ions with the chain, resulting in sliding of the ion along the chain backbone.[42] This relative motion where the chain drags the adsorbed ions with it can be visualized in Supporting Information-Movie S2. The inset of Figure 8 displays μ_c normalized w.r.t. to a free ion's mobility $\mu^0 \approx 0.015$ in response to varying fields and frequencies. We observe that with increasing field strength, initially, mobility increases, followed by a decrease beyond the threshold field $E^2/\nu \approx 10^3$. It is important to note that the adsorbed ion's mobility exhibits a pronounced departure from its response in the DC field, where a monotonic increase is seen. Based on prior studies[42] probing counterions' dynamical coupling with PE under DC fields, a few speculative arguments can be made. The increase in electrostatic coupling of the ion-chain duo due to inherent chain foldings might cause a decrease in an ion's mobility. Apart from this conformational obstruction, strong asymmetric polarization of condensed counterions gives rise to intrinsic fields,[79] counter-acting the external field. The latter is addressed in the subsequent subsection.

3.5. Polarization. The polarizability of PE in bulk predominantly comes from the distribution of ions in the chain's vicinity.[80] Additionally, subjection to external field leads to stronger anisotropic polarization along the chain backbone due to a resultant ion cloud shift. To provide insights into the local polarization, we first present the evolution of charge distribution $\rho(\delta r_x, t)$ over a half cycle w.r.t. the center-of-mass for different time instances $t = 0, \tau_\nu/10, \tau_\nu/5, 3\tau_\nu/10$, and $\tau_\nu/2$ in the compressed regime; see the inset of Figure 9. Here, $\delta r_x = r^x - R_{cm}^x$ is the relative position of ion w.r.t. the center of mass.

A huge asymmetry in $\rho(\delta r_x, t)$ is observed at the terminal ends, where the positive peak corresponds to the accumulation of counterions in response to the field to one side, while the negative peak results from the desorption of ions from the fragment of the chain at the other side. This asymmetry is clearly visible in the Supporting Information Movie S1.[53] Additionally, a secondary peak indicates overlapping regions of the chain.

The ion cloud shifts from one end to the other end at the field reversal; see the inset of Figure 9 at $t = \tau_\nu/2$. Consequently, the
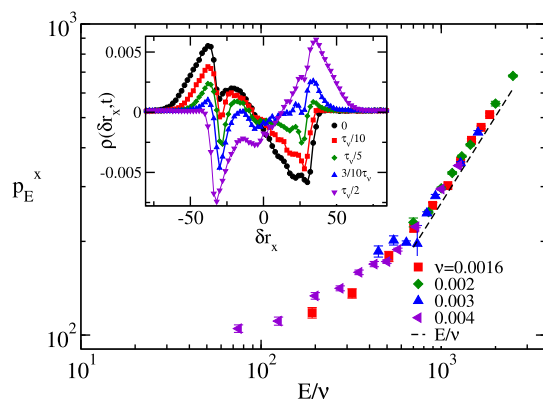
Figure 9. Average polarization $p_E{}^x$ as a function E/ν; the dashed line shows a linear increase in $p_E{}^x$ in the range of $E/\nu > 700$. The inset shows total charge density distribution $\rho(\delta r_x, t)$, where $\delta r_x = r^x - R_{cm}{}^x$ along the channel axis of the monomer−counterion duo relative to the center-of-mass of the chain at time instances $t = 0$, $\tau_\nu/10$, $\tau_\nu/5$, $3\tau_\nu/10$, and $\tau_\nu/2$ for $\nu = 0.002$.

induced dipole moment reorients along the preferred field direction. This is corroborated from the dipole reorientation expressed in terms of the correlation of polarization $C_{px}(t)$. For that, instantaneous values of polarization are taken as

$$\mathbf{p}_E{}^i(t) = \frac{1}{V}\left[\sum_i q_i(\mathbf{r}_i - \mathbf{r}_{cm}) + \sum_j q_j^c(\mathbf{r}_j^c - r_{cm})\right].$$ [17,20,41] Here,

all the ions are considered in the wake of overall ion cloud reconfiguration. Interestingly, the polarization reorientation exhibits a symmetric curve in the region $E > E_c$, inferring that the chain−counterion duo completely reconfigure in the phase with the electric field in every half cycle, see Supporting Information Figure S3.[53] However, for $E < E_c$, the ion cloud is unable to reorient in the exposed time-scale, resulting in weak asymmetric polarization $p_E{}^x$.

Now, we emphasize the role of condensed counterions in the polarization of the chain. For that, we estimate the root-mean-square polarization of the chain-condensed ion duo. The quantified values of $p_E{}^x$ remarkably superimpose onto a master curve if scaled with E/ν as shown in Figure 9. Surprisingly, in the compressed regime, despite the strong electric field, the average polarization shows a linear behavior with constant polarizability as displayed by a dashed line in the limit of $E/\nu > 700$. Despite the alternating nature of the applied field, under considerably high fields, the PE chain and the counterion cloud quickly reconfigure prior to the field switch. As a result, the linearity in polarization in this regime can be perceived as a direct outcome of a strong field-orchestrated distortion of the ion cloud. However, in the weak field limit, this direct effect of the field is overshadowed by the dominant diffusive nature of ions, leading to pronounced coupling of ions with local fields present in the chain's vicinity. Because of this weak influence of field over ions, polarization varies sub-linearly with E in this regime.

4. CONCLUSIONS AND DISCUSSION

Using molecular dynamic simulations, we provide compelling evidence of AC field-induced compression of a confined PE chain. We observe that for a narrow range of frequencies, beyond a threshold field strength, the chain undergoes an anisotropic compression manifested in terms of multiple hairpin bends.[26,45] One of our key findings elucidates the indispensability of HIs in the collapse mechanism, where a chain in the absence of HIs exhibits monotonic stretching and is devoid of any folding. This

proposition can be extended to the earlier cases of DNA collapse in nanochannels,[35,36] where intra-chain hydrodynamic coupling was speculated to have a secondary role. Further, based on prior studies, where inhomogeneous hydrodynamic drag along the chain backbone under high fields leads to bending and alignment in elastic rods,[66,67,81] it can be fairly argued that HIs are precursors to these hairpin bends.

Further, we investigated the role of confinement, where we found that with the extent of spatial constriction becoming comparable to the chain size in bulk, non-monotonicity in the chain response diminishes. This, followed by a complete monotonic stretch seen in bulk, unveils the pivotal involvement of confinement in the chain folding mechanism. Although our results correspond to shorter chains relative to DNA collapse experiments, despite that they capture most of their characteristic features, particularly the chain's fractional compression under an AC field[34−36] and its qualitative variation with parameters such as field strength, frequency, confinement, and viscosity (see Supporting Information Figure S4[53]).

Additionally, the frequency dependence of DNA collapse in the experiments has been speculated to be a consequence of certain intrinsic timescales associated with the chain and ions coinciding with the time-period of the applied field. To corroborate this contention, we primarily investigate the intrinsic relaxation of the chain in the DC field. The relaxation time $\tau_{R_e}(E)$ corresponding to the fluctuation of end-to-end distance in the DC field undergoes a sharp decrease at $E_{dc}^* \approx 1.1$ as shown in Supporting Information Figure S1b.[53] With the time-period of the electric field τ_ν spanning the range $20-1000$, the following inferences can be made here regarding the chain's structural response; (1) $\tau_\nu \gg \tau_{R_e}(E)$, chain stretches as in DC owing to complete chain relaxation.[40] (2) In the range of $\sigma^2/D_0 < \tau_\nu < \tau_{R_e}(E)$, the local segmental alignment induces partial stretching as reflected in the case of $E < E_{dc}^*$, and further if $\tau_\nu \to \sigma^2/D_0 \approx 32$ (at $\nu = 0.05$), the chain is weakly perturbed. (3) For $\tau_\nu \approx \tau_{R_e}(E)$, the field strongly influences the overall chain's relaxation and evidently, this coincides with the $E > E_{dc}^*$ regime, where collapse of the chain is observed.

Further, in an attempt to address the relaxation time associated with the ion cloud, we compare diffusive length-scale of an ion, that is, $\delta_D = \sqrt{\frac{2D_a}{\nu}}$ and amplitude of oscillation of the adsorbed counterion $\delta_\mu = \mu_c E/\nu$ in response to the field.[36,69] The adsorbed ion diffusivity is taken as $D_a \approx 0.01$ and mobility is $\mu_c \approx 0.0037$. Typical values of (δ_D, δ_μ) at the critical field $E_c{}^2/\nu = 10^3$ are $(3.1, 2.6)$, $(2.2, 1.9)$, and $(1.4, 1.2)$ for frequencies $\nu = 0.002$, 0.004, and 0.01, respectively. This suggests that at $E = E_c$, δ_D is comparable to δ_μ. Once $\delta_D > \delta_\mu$ for $E < E_c$, the ion reconfiguration is predominantly governed by diffusive behavior, which results in asymmetric polarization of the chain. On the other hand, for $E > E_c$ where $\delta_D \leq \delta_\mu$, the ions drift larger distances, surpassing the diffusive length scales, causing polarization in sync with the time-period of the applied field. This strong field-orchestrated ion reconfiguration further confirms the observed linear behavior of polarization $p_E{}^x \sim E$ in the limit of $E > E_c$ (see Figure 9). Hence, it can be inferred that the collapse of PE in an AC field is a quintessential hydrodynamically driven phenomenon that encompasses multitudes of system-relevant length- and time-scales, particularly the chain's relaxation time $\tau_{R_e}(E)$, the polarization length-scale of ions δ_μ exhibiting remarkable coupling with the time-period of

the applied field. The closer insights gained here can be a big leap in intuitive and conceptual build-up of such a complex phenomenon.

Finally, the nature of PE collapse in AC shares semblance to Odijk's backfoldings.[26,27,45,61,70] In equilibrium, these thermally activated backfoldings appear in a narrow window of $2R_p \sim l_p$. However, field-induced alignment and resultant enhanced global stiffness lead to the formation of such hairpins even in the weak confinement limit, that is, $2R_p \gg l_p$. Additionally, the obtained non-monotonic structural response of the chain can be captured in terms of hairpin variables and local chain alignment. Our analysis reveals that in the compression regime, growth of alignment parameter m is dictated by a power law expressed as $1 - m \sim (E/\nu)^{-2/5}$. Similarly, the global persistence length g also grows, showing a power-law variation. Further, these findings are especially conducive in identifying regimes pertaining to E and ν in dielectrophoresis experiments,[82−85] where backfoldings can obstruct the desired linearization of the DNA molecule.

Additionally, relaxation and unfolding of these folded domains under constant force may further shed light on the associated time- and length-scales of the chain.[69,86−90] Further, our study has broader applications in the lab on chip experiments, where field-induced effects can be exploited to elucidate several physical aspects of biopolymers such as knotting, entanglements, looping, gene regulation, chromosome localization in confined environments, and so forth.[34,85,91,92]

■ ASSOCIATED CONTENT

Ⓢ Supporting Information

The Supporting Information is available free of charge at https://pubs.acs.org/doi/10.1021/acs.macromol.1c00637.

> Detailed description of the MPC approach used for solvent dynamics, quantification of intrinsic time scales of the system, hairpin length variation, polarization relaxation of the ion cloud, and PE structural response with varying viscosity (PDF)

> Dynamics of the PE and ions subjected to an AC field under certain conditions in the compression regime (MP4)

> Dynamics of the PE and ions subjected to an AC field under certain conditions in the stretching regime (MP4)

■ AUTHOR INFORMATION

Corresponding Authors

Keerthi Radhakrishnan − *Department of Physics, Indian Institute of Science Education and Research Bhopal, Bhopal 462066 Madhya Pradesh, India*; Email: keerthirk@iiserb.ac.in

Sunil P. Singh − *Department of Physics, Indian Institute of Science Education and Research Bhopal, Bhopal 462066 Madhya Pradesh, India*; Ⓞ orcid.org/0000-0002-1179-9247; Email: spsingh@iiserb.ac.in

Complete contact information is available at:
https://pubs.acs.org/10.1021/acs.macromol.1c00637

Notes

The authors declare no competing financial interest.

■ ACKNOWLEDGMENTS

■ REFERENCES

(1) Kong, C. Y.; Muthukumar, M. Modeling of polynucleotide translocation through protein pores and nanotubes. *Electrophoresis* **2002**, *23*, 2697−2703.

(2) Muthukumar, M.; Kong, C. Simulation of polymer translocation through protein channels. *Proc. Natl. Acad. Sci. U.S.A.* **2006**, *103*, 5273−5278.

(3) Venkatesan, B. M.; Bashir, R. Nanopore sensors for nucleic acid analysis. *Nat. Nanotechnol.* **2011**, *6*, 615−624.

(4) Derrington, I. M.; Butler, T. Z.; Collins, M. D.; Manrao, E.; Pavlenok, M.; Niederweis, M.; Gundlach, J. H. Nanopore DNA sequencing with MspA. *Proc. Natl. Acad. Sci. U.S.A.* **2010**, *107*, 16060−16065.

(5) Branton, D.; Deamer, D. W.; Marziali, A.; Bayley, H.; Benner, S. A.; Butler, T.; Di Ventra, M.; Garaj, S.; Hibbs, A.; Huang, X.; et al. The potential and challenges of nanopore sequencing. *Nat. Biotechnol.* **2008**, *26*, 1146.

(6) Han, J.; Craighead, H. G. Separation of long DNA molecules in a microfabricated entropic trap array. *Science* **2000**, *288*, 1026−1029.

(7) Muthukumar, M. *Polymer Translocation*; Taylor & Francis US, 2011.

(8) Benner, S.; Chen, R. J. A.; Wilson, N. A.; Abu-Shumays, R.; Hurt, N.; Lieberman, K. R.; Deamer, D. W.; Dunbar, W. B.; Akeson, M. Sequence-specific detection of individual DNA polymerase complexes in real time using a nanopore. *Nat. Nanotechnol.* **2007**, *2*, 718−724.

(9) Chen, P.; Gu, J.; Brandin, E.; Kim, Y.-R.; Wang, Q.; Branton, D. Probing single DNA molecule transport using fabricated nanopores. *Nano Lett.* **2004**, *4*, 2293−2298.

(10) Vodyanoy, I.; Bezrukov, S. M. Sizing of an ion pore by access resistance measurements. *Biophys. J.* **1992**, *62*, 10.

(11) Kasianowicz, J. J.; Brandin, E.; Branton, D.; Deamer, D. W. Characterization of individual polynucleotide molecules using a membrane channel. *Proc. Natl. Acad. Sci. U.S.A.* **1996**, *93*, 13770−13773.

(12) Jeon, B.-j.; Muthukumar, M. Polymer capture by α-hemolysin pore upon salt concentration gradient. *J. Chem. Phys.* **2014**, *140*, 015101.

(13) Wong, C. T. A.; Muthukumar, M. Polymer translocation through α-hemolysin pore with tunable polymer-pore electrostatic interaction. *J. Chem. Phys.* **2010**, *133*, 045101.

(14) Huang, L. R.; Cox, E. C.; Austin, R. H.; Sturm, J. C. Tilted Brownian ratchet for DNA analysis. *Anal. Chem.* **2003**, *75*, 6963−6967.

(15) Alexander-Katz, A.; Schneider, M. F.; Schneider, S. W.; Wixforth, A.; Netz, R. R. Shear-flow-induced unfolding of polymeric globules. *Phys. Rev. Lett.* **2006**, *97*, 138101.

(16) Hoagland, D. A.; Arvanitidou, E.; Welch, C. Capillary electrophoresis measurements of the free solution mobility for several model polyelectrolyte systems. *Macromolecules* **1999**, *32*, 6180−6190.

(17) Frank, S.; Winkler, R. G. Polyelectrolyte electrophoresis: Field effects and hydrodynamic interactions. *Europhys. Lett.* **2008**, *83*, 38004.

(18) Frank, S.; Winkler, R. G. Mesoscale hydrodynamic simulation of short polyelectrolytes in electric fields. *J. Chem. Phys.* **2009**, *131*, 234905.

(19) Grass, K.; Böhme, U.; Scheler, U.; Cottet, H.; Holm, C. Importance of Hydrodynamic Shielding for the Dynamic Behavior of Short Polyelectrolyte Chains. *Phys. Rev. Lett.* **2008**, *100*, 096104.

(20) Grass, K.; Holm, C. Polyelectrolytes in electric fields: measuring the dynamical effective charge and effective friction. *Soft Matter* **2009**, *5*, 2079.

(21) Schlagberger, X.; Netz, R. R. Anomalous polymer sedimentation far from equilibrium. *Phys. Rev. Lett.* **2007**, *98*, 128301.

(22) Singh, S. P.; Gompper, G.; Winkler, R. G. Steady state sedimentation of ultrasoft colloids. *J. Chem. Phys.* **2018**, *148*, 084901.

(23) Jonsson, M.; Jacobsson, U.; Takahashi, M.; Nordén, B. Orientation of large DNA during free solution electrophoresis studied by linear dichroism. *J. Chem. Soc., Faraday Trans.* **1993**, *89*, 2791−2798.

(24) Netz, R. R. Nonequilibrium unfolding of polyelectrolyte condensates in electric fields. *Phys. Rev. Lett.* **2003**, *90*, 128104.

(25) Singh, S. P.; Muthukumar, M. Electrophoretic mobilities of counterions and a polymer in cylindrical pores. *J. Chem. Phys.* **2014**, *141*, 114901.

(26) Odijk, T. Scaling theory of DNA confined in nanochannels and nanoslits. *Phys. Rev. E: Stat., Nonlinear, Soft Matter Phys.* **2008**, *77*, 060901.

(27) Muralidhar, A.; Tree, D. R.; Dorfman, K. D. Backfolding of wormlike chains confined in nanochannels. *Macromolecules* **2014**, *47*, 8446−8458.

(28) Stein, D.; van der Heyden, F. H. J.; Koopmans, W. J. A.; Dekker, C. Pressure-driven transport of confined DNA polymers in fluidic channels. *Proc. Natl. Acad. Sci. U.S.A.* **2006**, *103*, 15853.

(29) Jendrejack, R. M.; Schwartz, D. C.; de Pablo, J. J.; Graham, M. D. Shear-induced migration in flowing polymer solutions: Simulation of long-chain DNA in microchannels. *J. Chem. Phys.* **2004**, *120*, 2513.

(30) Jendrejack, R. M.; Dimalanta, E. T.; Schwartz, D. C.; Graham, M. D.; de Pablo, J. J. DNA dynamics in a microchannel. *Phys. Rev. Lett.* **2003**, *91*, 038102.

(31) Chelakkot, R.; Winkler, R. G.; Gompper, G. Migration of semiflexible polymers in microcapillary flow. *Europhys. Lett.* **2010**, *91*, 14001.

(32) Steinhauser, D.; Köster, S.; Pfohl, T. Mobility gradient induces cross-streamline migration of semiflexible polymers. *ACS Macro Lett.* **2012**, *1*, 541−545.

(33) Hickey, O. A.; Holm, C. Electrophoretic mobility reversal of polyampholytes induced by strong electric fields or confinement. *J. Chem. Phys.* **2013**, *138*, 194905.

(34) Tang, J.; Du, N.; Doyle, P. S. Compression and self-entanglement of single DNA molecules under uniform electric field. *Proc. Natl. Acad. Sci. U.S.A.* **2011**, *108*, 16153−16158.

(35) Zhou, C.; Riehn, R. Collapse of DNA under alternating electric fields. *Phys. Rev. E: Stat., Nonlinear, Soft Matter Phys.* **2015**, *92*, 012714.

(36) Zhou, C.; Reisner, W. W.; Staunton, R. J.; Ashan, A.; Austin, R. H.; Riehn, R. Collapse of DNA in AC electric fields. *Phys. Rev. Lett.* **2011**, *106*, 248103.

(37) Ueda, M.; Oana, H.; Baba, Y.; Doi, M.; Yoshikawa, K. Electrophoresis of long DNA molecules in linear polyacrylamide solutions. *Biophys. Chem.* **1998**, *71*, 113−123.

(38) Ueda, M. Dynamics of long DNA confined by linear polymers. *J. Biochem. Biophys. Methods* **1999**, *41*, 153−165.

(39) Kaji, N.; Ueda, M.; Baba, Y. Stretching of megabase-sized deoxyribonucleic acid molecules by tuning electric-field frequency. *Appl. Phys. Lett.* **2003**, *83*, 3413−3415.

(40) Liu, H.; Zhu, Y.; Maginn, E. Molecular Simulation of Polyelectrolye Conformational Dynamics under an AC Electric Field. *Macromolecules* **2010**, *43*, 4805−4813.

(41) Hsiao, P.-Y.; Wei, Y.-F.; Chang, H.-C. Unfolding collapsed polyelectrolytes in alternating-current electric fields. *Soft Matter* **2011**, *7*, 1207−1213.

(42) Netz, R. R. Polyelectrolytes in Electric Fields. *J. Phys. Chem. B* **2003**, *107*, 8208−8217.

(43) Bruinsma, R. F.; Riehn, R. DNA Condensation by Field-Induced Non-Equilibrium Noise. *ChemPhysChem* **2009**, *10*, 2871−2875.

(44) Isambert, H.; Ajdari, A.; Viovy, J.-L.; Prost, J. Electro-hydrodynamic Patterns in Charged Colloidal Solutions. *Phys. Rev. Lett.* **1997**, *78*, 971−974.

(45) Odijk, T. DNA confined in nanochannels: Hairpin tightening by entropic depletion. *J. Chem. Phys.* **2006**, *125*, 204904.

(46) Arnold, A.; Holm, C. MMM2D: A fast and accurate summation method for electrostatic interactions in 2D slab geometries. *Comput. Phys. Commun.* **2002**, *148*, 327−348.

(47) Spohr, E. Effect of electrostatic boundary conditions and system size on the interfacial properties of water and aqueous solutions. *J. Chem. Phys.* **1997**, *107*, 6342−6348.

(48) Yeh, I.-C.; Berkowitz, M. L. Ewald summation for systems with slab geometry. *J. Chem. Phys.* **1999**, *111*, 3155−3162.

(49) Arnold, A.; Holm, C. MMM1D: A method for calculating electrostatic interactions in one-dimensional periodic geometries. *J. Chem. Phys.* **2005**, *123*, 144103.

(50) Lekner, J. Summation of Coulomb fields in computer-simulated disordered systems. *Phys. A* **1991**, *176*, 485−498.

(51) Deserno, M.; Holm, C. How to mesh up Ewald sums. II. An accurate error estimate for the particle-particle-particle-mesh algorithm. *J. Chem. Phys.* **1998**, *109*, 7694−7701.

(52) Deserno, M.; Holm, C. How to mesh up Ewald sums. I. A theoretical and numerical comparison of various particle mesh routines. *J. Chem. Phys.* **1998**, *109*, 7678−7693.

(53) Radhakrishnan, K.; Singh, S. P. Conformational dynamics of a confined Polyelectrolyte under AC field. Supporting Material 2020.

(54) Kapral, R. Multiparticle collision dynamics: Simulation of complex systems on mesoscales. *Adv. Chem. Phys.* **2008**, *140*, 89.

(55) Gompper, G.; Ihle, T.; Kroll, D.; Winkler, R. Multi-particle collision dynamics: A particle-based mesoscale simulation approach to the hydrodynamics of complex fluids. *Advanced Computer Simulation Approaches for Soft Matter Sciences III*; Springer, 2009; pp 1−87.

(56) Lamura, A.; Gompper, G.; Ihle, T.; Kroll, D. M. Multi-particle collision dynamics: Flow around a circular and a square cylinder. *Europhys. Lett.* **2001**, *56*, 319.

(57) Huang, C. C.; Chatterji, A.; Sutmann, G.; Gompper, G.; Winkler, R. G. Cell-level canonical sampling by velocity scaling for multiparticle collision dynamics simulations. *J. Comp. Physiol.* **2010**, *229*, 168.

(58) Huang, C.-C.; Gompper, G.; Winkler, R. G. Non-equilibrium relaxation and tumbling times of polymers in semidilute solution. *J. Phys.: Condens. Matter* **2012**, *24*, 284131.

(59) Allen, M. P.; Tildesley, D. J. *Computer Simulation of Liquids*; Clarendon Press: Oxford, 1987.

(60) Frenkel, D.; Smit, B. *Understanding Molecular Simulation: From Algorithms to Applications*; Elsevier, 2001; Vol. 1.

(61) Reisner, W.; Morton, K. J.; Riehn, R.; Wang, Y. M.; Yu, Z.; Rosen, M.; Sturm, J. C.; Chou, S. Y.; Frey, E.; Austin, R. H. Statics and dynamics of single DNA molecules confined in nanochannels. *Phys. Rev. Lett.* **2005**, *94*, 196101.

(62) Daoud, M.; De Gennes, P. G. Statistics of macromolecular solutions trapped in small pores. *J. Phys.* **1977**, *38*, 85−93.

(63) Wang, Y.; Tree, D. R.; Dorfman, K. D. Simulation of DNA extension in nanochannels. *Macromolecules* **2011**, *44*, 6594−6604.

(64) Reisner, W.; Pedersen, J. N.; Austin, R. H. DNA confinement in nanochannels: physics and biological applications. *Rep. Prog. Phys.* **2012**, *75*, 106601.

(65) Das, A. K.; Hsiao, P.-Y. Charged dendrimers under the action of AC electric fields: Breathing characteristics of molecular size, polarizations, and ion distributions. *J. Chem. Phys.* **2015**, *142*, 084902.

(66) Schlagberger, X.; Netz, R. R. Anomalous birefringence and polarizability saturation of charged elastic rods: Field-strength, salt and finite-concentration effects. *Europhys. Lett.* **2008**, *83*, 36003.

(67) Cosentino Lagomarsino, M.; Pagonabarraga, I.; Lowe, C. P. Hydrodynamic induced deformation and orientation of a microscopic elastic filament. *Phys. Rev. Lett.* **2005**, *94*, 148104.

(68) Sendner, C.; Netz, R. R. Single flexible and semiflexible polymers at high shear: Non-monotonic and non-universal stretching response. *Eur. Phys. J. E: Soft Matter Biol. Phys.* **2009**, *30*, 75−81.

(69) Cohen, A. E. Force-extension curve of a polymer in a high-frequency electric field. *Phys. Rev. Lett.* **2003**, *91*, 235506.

(70) Dai, L.; Ng, S. Y.; Doyle, P. S.; van der Maarel, J. R. C. Conformation model of back-folding and looping of a single DNA molecule confined inside a nanochannel. *ACS Macro Lett.* **2012**, *1*, 1046−1050.

(71) Tree, D. R.; Wang, Y.; Dorfman, K. D. Extension of DNA in a nanochannel as a rod-to-coil transition. *Phys. Rev. Lett.* **2013**, *110*, 208103.

(72) Raphael, E.; Pincus, P. Scaling theory of polymer solutions trapped in small pores: the θ-solvent case. *J. Phys. II* **1992**, *2*, 1341−1344.

(73) Odijk, T. The statistics and dynamics of confined or entangled stiff polymers. *Macromolecules* **1983**, *16*, 1340−1344.

(74) Muralidhar, A.; Dorfman, K. D. Backfolding of DNA confined in nanotubes: Flory theory versus the two-state cooperativity model. *Macromolecules* **2016**, *49*, 1120−1126.

(75) Spakowitz, A. J.; Wang, Z.-G. Semiflexible polymer solutions. I. Phase behavior and single-chain statistics. *J. Chem. Phys.* **2003**, *119*, 13113−13128.

(76) Tkachenko, A.; Rabin, Y. Coupling between thermodynamics and conformations in wormlike polymer nematics. *Macromolecules* **1995**, *28*, 8646−8656.

(77) Liu, S.; Muthukumar, M. Langevin dynamics simulation of counterion distribution around isolated flexible polyelectrolyte chains. *J. Chem. Phys.* **2002**, *116*, 9975−9982.

(78) Winkler, R. G.; Gold, M.; Reineker, P. Collapse of polyelectrolyte macromolecules by counterion condensation and ion pair formation: a molecular dynamics simulation study. *Phys. Rev. Lett.* **1998**, *80*, 3731.

(79) Manning, G. S. Limiting laws and counterion condensation in polyelectrolyte solutions I. Colligative properties. *J. Chem. Phys.* **1969**, *51*, 924−933.

(80) Mohanty, U.; Zhao, Y. Polarization of counterions in polyelectrolytes. *Biopolymers* **1996**, *38*, 377−388.

(81) Manghi, M.; Schlagberger, X.; Kim, Y.-W.; Netz, R. R. Hydrodynamic effects in driven soft matter. *Soft Matter* **2006**, *2*, 653−668.

(82) Asbury, C. L.; Van Den Engh, G. Trapping of DNA in nonuniform oscillating electric fields. *Biophys. J.* **1998**, *74*, 1024−1030.

(83) Washizu, M.; Kurosawa, O.; Arai, I.; Suzuki, S.; Shimamoto, N. Applications of electrostatic stretch-and-positioning of DNA. *IEEE Trans. Ind. Appl.* **1995**, *31*, 447−456.

(84) Dewarrat, F.; Calame, M.; Schönenberger, C. Orientation and positioning of DNA molecules with an electric field technique. *Single Mol.* **2002**, *3*, 189−193.

(85) Mahshid, S.; Lu, J.; Abidi, A. A.; Sladek, R.; Reisner, W. W.; Ahamed, M. J. Transverse dielectrophoretic-based DNA nanoscale confinement. *Sci. Rep.* **2018**, *8*, 5981.

(86) Levy, S. L.; Mannion, J. T.; Cheng, J.; Reccius, C. H.; Craighead, H. G. Entropic unfolding of DNA molecules in nanofluidic channels. *Nano Lett.* **2008**, *8*, 3839−3844.

(87) Radhakrishnan, K.; Singh, S. P. Force driven transition of a globular polyelectrolyte. *J. Chem. Phys.* **2019**, *151*, 174902.

(88) Frisch, T.; Verga, A. Unwinding globules under tension and polymer collapse. *Phys. Rev. E: Stat., Nonlinear, Soft Matter Phys.* **2002**, *65*, 041801.

(89) Cooke, I. R.; Williams, D. R. M. Stretching polymers in poor and bad solvents: Pullout peaks and an unraveling transition. *Europhys. Lett.* **2003**, *64*, 267.

(90) Gunari, N.; Balazs, A. C.; Walker, G. C. Force-induced globule-coil transition in single polystyrene chains in water. *J. Am. Chem. Soc.* **2007**, *129*, 10046−10047.

(91) Reisner, W.; Larsen, N. B.; Silahtaroglu, A.; Kristensen, A.; Tommerup, N.; Tegenfeldt, J. O.; Flyvbjerg, H. Single-molecule denaturation mapping of DNA in nanofluidic channels. *Proc. Natl. Acad. Sci. U.S.A.* **2010**, *107*, 13294−13299.

(92) Zhang, C.; Jiang, K.; Liu, F.; Doyle, P. S.; van Kan, J. A.; van der Maarel, J. R. C. A nanofluidic device for single molecule studies with in situ control of environmental solution conditions. *Lab Chip* **2013**, *13*, 2821−2826.